Two-Dimensional Nonlinear Thouless Pumping of Matter Waves

Qidong Fu,[1] Peng Wang,[1] Yaroslav V. Kartashov,[2] Vladimir V. Konotop,[3] and Fangwei Ye[1,*]
[1]School of Physics and Astronomy, Shanghai Jiao Tong University, Shanghai 200240, China
[2]Institute of Spectroscopy, Russian Academy of Sciences, Troitsk, Moscow Region 108840, Russia
[3]Departamento de Física and Centro de Física Teórica e Computacional, Faculdade de Ciências, Universidade de Lisboa, Campo Grande, Ed. C8, Lisboa 1749-016, Portugal

(Received 2 May 2022; accepted 12 September 2022; published 24 October 2022)

We consider theoretically the nonlinear quantized Thouless pumping of a Bose-Einstein condensate loaded in two-dimensional dynamical optical lattices. We encountered three different scenarios of the pumping: a quasilinear one occurring for gradually dispersing wave packets, transport carried by a single two-dimensional soliton, and a multisoliton regime when the initial wave packet splits into several solitons. The scenario to be realized depends on the number of atoms in the initial wave packet and on the strength of the two-body interactions. The magnitude and direction of the displacement of a wave packet are determined by Chern numbers of the populated energy bands and by the interband transitions induced by two-body interactions. As a case example we explore a separable potential created by optical lattices whose constitutive sublattices undergo relative motion in the orthogonal directions. For such potentials, obeying parity-time symmetry, fractional Chern numbers, computed over half period of the evolution, acquire relevance. We focus mainly on solitonic scenarios, showing that one-soliton pumping occurs at relatively small as well as at sufficiently large amplitudes of the initial wave packet, while at intermediate amplitudes the transport is multisolitonic. We also describe peculiarities of the pumping characterized by two different commensurate periods of the modulations of the lattices in the orthogonal directions.

DOI: 10.1103/PhysRevLett.129.183901

Since its discovery by Thouless [1], quantized transport has been the focus of extensive studies for electrons in condensed matter [2–4], in spinor systems [5], fermionic [6–8] and bosonic [9,10] atomic gasses, in photonic [11–13] and acoustic [14] systems, and in plasmonic waveguides [15]. Originally quantized transport (alias Thouless pumping) was studied in one-dimensional (1D) linear systems. Experimental observations of this phenomenon in optical and atomic systems have triggered investigations of the impact of the space dimension and of the nonlinearity on transport.

One can distinguish two 2D implementations of quantized transport. The first one, that has received the most attention so far, is motivated by the intimate relation between quantized transport and different Hall effects. Such transport occurs along boundaries of finite 2D structures and is carried by the boundary modes [12]. Being strongly confined to the boundaries, this mechanism is quasi-one-dimensional in real space, although it may require the use of effective multidimensional spaces for its analytical description. The second implementation is the transport carried by bulk modes (in a formally unlimited potential). In addition to a quantized one-cycle displacement such transport is characterized by a quantized angle determining the direction of motion. The latter setting was implemented experimentally with a Bose-Einstein condensate (BEC) in an optical superlattice [9] and in tilted moiré lattices [16]. Two-dimensional Thouless pumping of ultracold fermions was studied in [17].

It was established theoretically [18–21] and confirmed experimentally [22], that in 1D systems nonlinearity (originated by two-body interactions in atomic gasses and by the Kerr effect in optical waveguides) can lead to breakup of the pumping. On the other hand, the nonlinearity sustains robust transport against disorder [23], allows one to achieve inversion of the pumping direction [19], and enables fractional pumping [8,24]. Quantized transport can also be induced by interactions [25].

One-dimensional Thouless pumping of large-amplitude wave packets in BECs with a negative scattering length occurs in a form of solitons, whose one-cycle displacement is determined by populations of several lowest bands varying due to interband tunneling and characterized by the *first* Chern numbers of the populated *linear* bands [19]. Thus, nonlinear quantized transport inherits the topological properties of the underlying linear system, while the nonlinearity controls the displacement through the coupling of populated bands.

In this Letter, we aim at considering quantized transport in a 2D BEC with a negative scattering length in the physical realization that goes far beyond the finite tight-binding model explored previously [20] and has features having no analogs in the continuous 1D systems [19]. Properties of pumping that cannot be observed in the

previous settings are as follows. First, a wave packet described by the 2D Gross-Pitaevskii equation (GPE) with attractive interactions may collapse if the number of atoms exceeds a specific value [26,27]. Second, while an optical lattice (OL) can in principle stabilize 2D solitons [28,29], it is not obvious *a priori* that such stabilization persists for high-amplitude wave packets evolving in dynamical OLs. Third, there is a threshold number of atoms required for soliton formation, i.e., for a solitonic transport. Consequently, the continuous model considered here reveals novel scenarios of nonlinear quantized transport carried either by a quasilinear wave packet, by a dynamically stable single soliton, or by several solitons emerging during the decay of the initial wave packet due to instability induced by interband tunneling. The nonlinearity determines which of these scenarios is realized, as well as the absolute value and direction of the one-cycle displacement. Furthermore, we report on peculiarities of pumping by lattices with different temporal periods in the orthogonal directions.

Consider a quasi-2D condensate described by the dimensionless GPE

$$i\frac{\partial\Psi}{\partial t}=-\frac{1}{2}\nabla^2\Psi+[V^x(x,t)+V^y(y,t)]\Psi-|\Psi|^2\Psi. \tag{1}$$

Here $\nabla=(\partial_x,\partial_y)$, $\boldsymbol{r}=(x,y)$ is measured in units of d/π where d is the smallest of the lattice constants, time t is measured in units of $md^2/(\pi^2\hbar)$, the amplitudes of the OL $V^\xi(\xi,t)=V^\xi(\xi+\pi,t)=V^\xi(\xi,t+T_\xi)$ (hereafter $\xi=x,y$) are given in units of $md^2/(\pi\hbar)^2$, $T_{x,y}$ are temporal periods which can be different but commensurate. The Ψ is normalized as $N\coloneqq\int|\Psi|^2d\boldsymbol{r}=\mathcal{N}(\pi/2)^{1/2}|a_s|/a_\perp$, where $\mathcal{N}$ is the total number of atoms, and $a_\perp$ is the condensate extension along the z direction (e.g., for a ^{7}Li BEC with $a_s\approx-1.43$ nm in a trap with $a_\perp\approx1$ μm the norm $N=1$ corresponds to $\mathcal{N}=558$ atoms). We assume that $T_x=nT_y$ where n is an integer, i.e., $T=T_x$ is the period of the 2D lattice.

Because of separability of the potential in Eq. (1) one can introduce 1D Hamiltonians $H^\xi=-(1/2)\partial_\xi^2+V^\xi(\xi,t)$ and consider the eigenvalue problems $H^\xi\varphi^\xi_{\alpha_\xi k_\xi}=\varepsilon^\xi_{\alpha_\xi k_\xi}(t)\varphi^\xi_{\alpha_\xi k_\xi}$ for the Bloch functions $\varphi^\xi_{\alpha_\xi k_\xi}=e^{ik_\xi\xi}u^\xi_{\alpha_\xi k_\xi}(\xi,t)$, where $u^\xi_{\alpha_\xi k_\xi}(\xi,t)=u^\xi_{\alpha_\xi k_\xi}(\xi+\pi,t)$, $k_\xi\in[-1,1)$, and α_ξ are the indices of the 1D bands. The spectrum of the full Hamiltonian $H=H^x+H^y$ is given by $\varepsilon_{\nu\boldsymbol{k}}(t)=\varepsilon^x_{\alpha_x k_x}(t)+\varepsilon^y_{\alpha_y k_y}(t)$, where $\boldsymbol{k}=(k_x,k_y)$ and ν is the index of 2D bands at $\boldsymbol{k}=\boldsymbol{0}$ and $t=0$. We restrict the consideration to potentials for which $\varepsilon_{\nu_1\boldsymbol{0}}(0)<\varepsilon_{\nu_2\boldsymbol{0}}(0)$ if $\nu_1<\nu_2$. Such a choice implies one-to-one correspondence $\nu\leftrightarrow(\alpha_x,\alpha_y)$, with $\nu=1$ corresponding to $(\alpha_x,\alpha_y)=(1,1)$. If no crossing of the 1D bands occurs at $t>0$, the labeling of $\varepsilon_{\nu\boldsymbol{k}}(t)$ by ν remains well defined at any t and $\boldsymbol{k}$. Now one can define Chern numbers of the 1D potentials:

$$C^\xi_{\alpha_\xi}(T_\xi)=\frac{i}{2\pi}\int_0^{T_\xi}dt\int_{-1}^{1}dk(\langle\partial_t u^\xi_{\alpha_\xi k}|\partial_k u^\xi_{\alpha_\xi k}\rangle-\langle\partial_k u^\xi_{\alpha_\xi k}|\partial_t u^\xi_{\alpha_\xi k}\rangle) \tag{2}$$

(here $\langle f|g\rangle\coloneqq\int_0^\pi\bar{f}(\xi)g(\xi)d\xi$ and an overbar denotes complex conjugation).

We characterize pumping by the displacement of the center of mass (c.m.) of the wave packet $\boldsymbol{\mathcal{R}}(t)=(1/N)\int_{\mathbb{R}^2}\boldsymbol{r}|\Psi|^2d^2r$. Defining 2D Wannier functions, $W^{\boldsymbol{n}}_\nu(\boldsymbol{r},t)=w^x_{\alpha_x n_x}(x,t)w^y_{\alpha_y n_y}(y,t)$ where $\boldsymbol{n}=(n_x,n_y)$, $n_{x,y}$ are integers, and $w^\xi_{\alpha_\xi n_\xi}(\xi,t)=(1/2)\int_{-1}^{1}\varphi^\xi_{\alpha_\xi k}(\xi,t)e^{-i\pi n_\xi k}dk$ are 1D Wannier functions [30,31]; for $N<N_{\rm cr}$, where $N_{\rm cr}$ is the critical number of atoms above which the initial wave packet collapses, we expand $\Psi(\boldsymbol{r},t)=\sqrt{N}\sum_{\nu=1}^{\infty}\times\sum_{\boldsymbol{n}}a^{\boldsymbol{n}}_\nu(t)W^{\boldsymbol{n}}_\nu(\boldsymbol{r},t)$. The coefficients $a^{\boldsymbol{n}}_\nu(t)$ are normalized $\sum_{\nu,\boldsymbol{n}}|a^{\boldsymbol{n}}_\nu|^2=1$. Using this expansion one can show that $\boldsymbol{\mathcal{R}}(t)=\boldsymbol{R}(t)+\boldsymbol{\eta}(t)+\boldsymbol{\zeta}(t)$ [32]. Here $\boldsymbol{R}(t)=(X(t),Y(t))=\sum_\nu\rho_\nu(X_{\alpha_x},Y_{\alpha_y})$ describes dynamics of the c.m. due to adiabatic change of the potential, $\rho_\nu(t)=\sum_{\boldsymbol{n}}|a^{\boldsymbol{n}}_\nu(t)|^2$ is the relative population of the νth band ($\sum_\nu\rho_\nu=1$), while $X_{\alpha_x}(t)=\int|w^x_{\alpha_x 0}|^2xdx$ and $Y_{\alpha_y}(t)=\int|w^y_{\alpha_y 0}|^2ydy$ are independent displacements (also known as polarizations [34]) along the x and y directions. The $\boldsymbol{\eta}(t)=\pi\sum_{\boldsymbol{n}}\eta^{\boldsymbol{n}}\boldsymbol{n}$, where $\eta^{\boldsymbol{n}}=\sum_\nu|a^{\boldsymbol{n}}_\nu|^2$, describes change of the c.m. position due to the tunneling between potential wells while $\boldsymbol{\zeta}(t)$ encompasses simultaneous spatial tunneling between minima of the potential accompanied by the interband transitions. Equations for $a^{\boldsymbol{n}}_\nu(t)$, as well as the explicit form of $\boldsymbol{\zeta}$ are given in [32]. While dispersive spreading of a small-amplitude wave packet can be a nonadiabatic process occurring faster than the motion of a c.m., the pumping still can be observed in this case. For a separable potential such a limit becomes a superposition of independent pumping along x and y directions determined by X_{α_x} and Y_{α_y}. In weakly nonlinear 1D systems the dispersive pumping was discussed in [19] (see also [32]).

Meantime, unlike in the cases of nonlinear pumping in a 1D GPE [19] and in a 2D finite discrete lattice [20], the domain of a quasilinear pumping cannot be reduced to zero, because solitons of the 2D GPE do not bifurcate from the linear modes. For a soliton of (1) to be created, the norm N must exceed some threshold value $N_{\rm th}$. Both $N_{\rm th}$ and $N_{\rm cr}$ depend on the specific parameters of the OL and in our case adiabatically vary in time. Therefore, these quantities are understood below as the maxima: $N_{\rm th,cr}=\max_t\{N_{\rm th,cr}(t)\}$, where $N_{\rm th,cr}(t)$ are the respective instantaneous values. At $N<N_{\rm th}$ the pumping is quasilinear. At $N_{\rm th}<N<N_{\rm cr}$ the attractive nonlinearity can sustain *stable* 2D solitons [35,36]. It turns out that in the solitonic regime two different scenarios occur: a single-soliton pumping and a multisoliton pumping. In the former case, when only one soliton is created, the tunneling between neighboring lattice

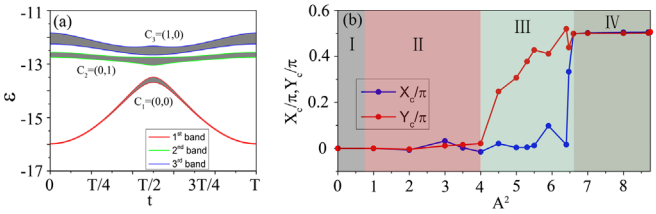

FIG. 1. (a) Evolution of 2D bands (grey domains with boundaries shown by color lines) over one cycle T of variation of the potential (4) with $\mathfrak{V}_x = 5$, $\mathfrak{V}_y = 4$, $\mathfrak{v}_x = 1.2$ and $\mathfrak{v}_y = 2$. Here $\nu = 1, 2, 3$ correspond to the pairs (1,1),(1,2),(2,1). The Chern numbers are indicated in the panel. (b) The (X_c, Y_c) obtained by the numerical simulations of Eq. (1) with $\Psi(\boldsymbol{r}, 0) = A\exp(-r^2/0.7^2)$ vs A^2, for $T = 100\pi$. Domains indicated by the encircled numbers correspond to different pumping regimes. The dots indicate amplitudes for which numerical data are obtained.

minima is suppressed by the attractive interatomic interactions. If also $\boldsymbol{\eta}(0) = \boldsymbol{\zeta}(0) = \mathbf{0}$, these quantities remain small at $t = T$ and tend to zero at $T \to \infty$ [32]. Below we consider wave packets initially centered at $\boldsymbol{\mathcal{R}}(0) = \mathbf{0}$, for which $\boldsymbol{\mathcal{R}}(T) \approx \boldsymbol{\mathcal{R}}(T)$. Then, since $X_{\alpha_x}(T_x) \approx \pi C^x_{\alpha_x}(T_x)$ and $Y_{\alpha_y}(T_y) \approx \pi C^y_{\alpha_y}(T_y)$, for quasilinear and single-soliton scenarios one can estimate $[\boldsymbol{\mathcal{R}}_T \coloneqq \boldsymbol{\mathcal{R}}(T)]$

$$\boldsymbol{\mathcal{R}}_T \approx \pi \sum_\nu \rho_\nu(T)\boldsymbol{C}_\nu, \qquad \boldsymbol{C}_\nu = (C^x_{\alpha_x}, nC^y_{\alpha_y}). \tag{3}$$

Four comments are in order. First, at $n > 1$ Eq. (3) does not allow for an equally accurate adiabatic description (formally valid for $T \to \infty$) of the displacements along x and y directions, since the latter undergoes n cycles. Second, $\boldsymbol{\mathcal{R}}_T$ includes the dependence on the band populations $\rho_\nu(T)$, that makes the nonlinear dynamics nonseparable. Third, as we show below, in some cases the formula (3) remains valid even at half-period $t = T/2$. Finally, transport may be accompanied by a nonadiabatic process of splitting of the initial wave packet into several solitons. Although then $\boldsymbol{\eta}(t)$ and $\boldsymbol{\zeta}(t)$ cannot be neglected, the approximation (3) remains meaningful for the interpretation of the physical results.

For the illustration of the general picture described above, we explore the potentials of the form $(\xi = x, y)$

$$V^\xi(\xi, t) = -\mathfrak{V}_\xi[\cos^2\xi + \mathfrak{v}_\xi\cos^2(2\xi - v_\xi t)], \tag{4}$$

where $\mathfrak{V}_\xi$ and $\mathfrak{v}_\xi$ are positive amplitudes, and $v_\xi = \pi/T_\xi$ are the velocities of the relative motion of the constitutive lattices. Starting with the case of equal periods $T_{x,y} = T$ (and, hence, $v_{x,y} = v = \pi/T$), in Fig. 1(a) we show an example of the three lowest 2D bands of the above lattice and their Chern numbers. All the results shown below are obtained for the Gaussian wave packet $\Psi_{\text{in}} = A\exp(-r^2/0.7^2)$ populating mainly the lowest band with $\boldsymbol{C}_1 = (0, 0)$ [Fig. 1(a)]. Respectively, in the quasilinear regime, corresponding to the parameter domain I in Figs. 1(b), no transport is observed, as predicted by (3). Interestingly, this is a quantum effect since in the classical limit a corresponding particle in the potential $V^x + V^y$ would display a half-period shift in each direction (see [32]).

The boundary between I and II domains at $A_{\text{th}} \approx 0.87$ corresponds to $N = N_{\text{th}} \approx 0.57$. Above this threshold a stable 2D soliton is created. For moderate nonlinearities $0.87 \lesssim A \lesssim 2$ in the entire domain II, one still does not observe appreciable c.m. shifts at $t = T$. This can be understood by considering the populations of the higher bands during one-cycle evolution plotted in Fig. 2(a). While weak nonlinearity couples the lowest (red line) band with the second (green line) and third (blue line) bands and tunneling does occur for $t < T$, the final distribution at $t = T$ is characterized by the dominant population of only the lowest band $[\rho_1(T) \approx 0.879$ in Fig. 2(a)]. Respectively, as predicted by $\boldsymbol{\mathcal{R}}_T \approx \mathbf{0}$ in (3), at $t = T$ the soliton is found

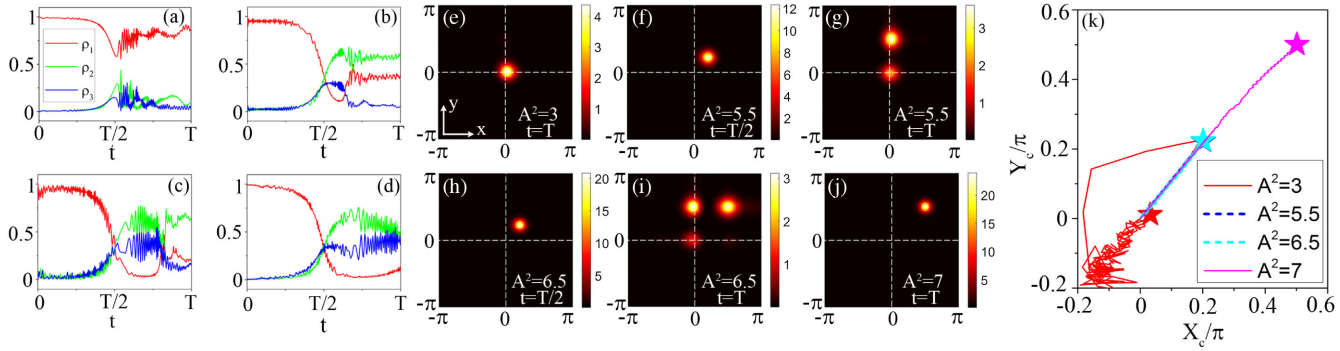

FIG. 2. Evolution of the population of the lowest bands for $A^2 = 3$ (a), 5.5 (b), 6.5 (c), and 7 (d). (e)–(j) Distributions $|\Psi|^2$ for the respective amplitudes at $t = T/2$ and $t = T$. The crossings of dashed lines indicate initial positions of the wave-packet centers. In (k) the trajectory of the c.m. for different initial amplitudes ended up in the locations shown by the stars at $t = T/2$ (dashed lines) and at $t = T$ (solid lines).

near the origin [Fig. 2(e)]. Meantime the trajectory at $0 < t < T$ appears very irregular [red line in Fig. 2(k)]. The observed long-time evolution is a numerical proof of the dynamical stability of a soliton.

Further increase of the input wave packet amplitude, corresponding to the domain III in Fig. 1(b), enhances the interband tunneling, especially around $t \approx T/2$ [Figs. 2(b) and 2(c)]. At that instant the 1D lattices in (4) are π-shifted and the amplitudes of the potentials V^{ξ} acquire their minimal values $\mathfrak{V}_{\xi}$. Inspecting band populations one observes that during the first half period most of the atoms are in the lowest linear band, while right after the instant $T/2$ most of the atoms tunnel to the second and third bands and new solitons are born. Now, the formula (3) is not applicable anymore at $t = T$, but it remains meaningful at $t = T/2$ (i.e., before the birth of new solitons) because the Chern numbers $C^{\xi}_{\alpha_{\xi}}(T_{\xi})$, considered as functions of T_{ξ}, remain topological quantities upon the replacement $T_{\xi} \to T_{\xi}/2$. Indeed, the Hamiltonians H^{ξ} with the potential (4) are parity-time symmetric, $[\mathcal{P}_{\xi}\mathcal{T}, H] = 0$ where the parity operators $\mathcal{P}_{\xi}$ change $\xi \to -\xi$ and $\mathcal{T}$ is the time reversal changing $t \to -t$ and performing complex conjugation. Bloch states of such Hamiltonians can also be chosen parity-time symmetric. Then, using the T_{ξ} periodicity of the potential $V^{\xi}(\xi, t)$, one can show [32] that $C^{\xi}_{\alpha_{\xi}}(T_{\xi}/2) = C^{\xi}_{\alpha_{\xi}}(T_{\xi})/2$, i.e., it is a (fractional) topological index and one can consider transport for $0 \le t \le T/2$. In Figs. 2(f) and 2(h) we show density distributions at $t = T/2$ for the cases that at $t = T$ have different numbers of newborn solitons. In both cases the initial wave packets have not undergone decay and have c.m. coordinates $\boldsymbol{\mathcal{R}}_{T/2} = (0.20, 0.22)\pi$. Moreover, the soliton trajectories in both cases are nearly the same: the blue and cyan dashed lines in Fig. 2(k) are indistinguishable. On the other hand, the half-period displacements predicted by Eq. (3) for band populations $(\rho_1, \rho_2, \rho_3) \approx (0.38, 0.35, 0.27)$ and (0.38,0.30,0.32) corresponding to the panels (f) and (h), are $\boldsymbol{\mathcal{R}}_{T/2} \approx (0.14, 0.18)\pi$ and $\boldsymbol{\mathcal{R}}_{T/2} \approx (0.16, 0.15)\pi$.

Thus, while the approximation (3) qualitatively explains the observed quantized transport, it underestimates the magnitude of the half-period displacement. This can be explained by two factors. First, (3) uses the normalization to N under the assumption that all atoms remain in the soliton at $t = T/2$, but in reality a small fraction of atoms from the initial Gaussian wave packet Ψ_{in} is always dispersed and does not contribute to the soliton. Thus, in practice a soliton has smaller "mass" N_s than the total norm, $N_s \lesssim N$, and a correction factor $f = N/N_s$ should be considered: $\boldsymbol{\mathcal{R}} \to f\boldsymbol{\mathcal{R}}$. In our simulations $f \approx 1.1$. Second, the dynamics of band populations is characterized by initial nonadiabatic evolution during the process of soliton formation [small-scale oscillations at $t \ll T$ in Figs. 2(b) and 2(c)]. Thus, effectively the adiabatic evolution "starts" at some $t_0 > 0$. To check this we considered $t_0 \approx 0.02T$ and computed $f\boldsymbol{\mathcal{R}}_{0.52T} \approx (0.17, 0.22)\pi$ and $f\boldsymbol{\mathcal{R}}_{0.52T} = (0.21, 0.23)\pi$ for the above cases, which is in excellent agreement with numerically obtained c.m. locations at $t = 0.52T$: $(0.21, 0.23)\pi$ and $(0.21, 0.22)\pi$.

Thus, the domain III is characterized by two different regimes: single-soliton transport until approximately $T/2$, when the soliton loses its stability because of enhanced interband tunneling [see Figs. 2(b) and 2(c)], followed by multisoliton transport. The output density distributions at $t = T$ are illustrated in Figs. 2(g) and 2(i). While the displacement at $T/2$ weakly depends on the input amplitude, at $t > T/2$ the dynamics crucially depends on A determining the number of emerging solitons [cf. panels (g) and (f)]. At $t = T$ all newborn solitons are centered in the vicinity of the points $(m, n)\pi/2$ where $m, n = 0, 1$.

A counterintuitive result is obtained upon further increase of the amplitude in the interval $6.6 \lessapprox A^2 \lessapprox 8.7$ [domain IV in Fig. 1(b)]. The initial wave packet evolves into a single large-amplitude soliton composed of atoms equally populating the topological second and third bands. At $t = T$ this two-band 2D soliton is encountered at the approximate position $(\pi/2, \pi/2)$ [Fig. 2(j)] in agreement with the formula (3). The right edge of the domain IV corresponds to the critical norm $N_{\text{cr}} \approx 6.69$ [$A^2_{\text{cr}} \approx 8.7$] above which the BEC collapses. The collapse occurs at a time much smaller than T [32]. When this happens the mean-field GPE does not describe all observed effects [37], requiring consideration of such effects as quantum fluctuations [38,39].

Nonlinear quantized transport in 2D allows one to consider nonequal periods of modulations along x and y directions. To explore this possibility we consider the potential (4) with $T_x = 2T_y = T$ ($v_y = 2v_x$). Figure 3 summarizes the results. For the chosen parameters the total second gap of the 2D lattice closes at certain instants of time [Fig. 3(a)], e.g., around $t = T/2$ the second 2D band acquires larger energy than the third one. At certain times we also observe shrinking of the first finite gap resulting in the enhancement of the interband tunneling [Figs. 3(c)–3(e)]. Meantime, the gaps of the constitutive 1D lattices (not shown here) remain permanently open. Therefore, the definition of the Chern numbers (2), indicated in Fig. 3(a), remain valid. Likewise, the formula (3) with $n = 2$ remains valid in the quasilinear regime [domain I in Fig. 3(b)] and in a single-soliton regime [domain II in Fig. 3(b)] that are analogous to respective regimes for equal periods. Upon increase of the amplitude of the initial wave packet we enter the domain, where the quantized transport is carried by several solitons. Now the first event of strong interband tunneling occurs approximately around $t \approx T/4$. For such an instant of time one cannot identify topological indices. Therefore the formula (3) can suggest only a qualitative interpretation of the results shown in Figs. 3(f) and 3(g). Since all atoms remain in the lowest two bands during the one-cycle evolution, the emerging solitons are

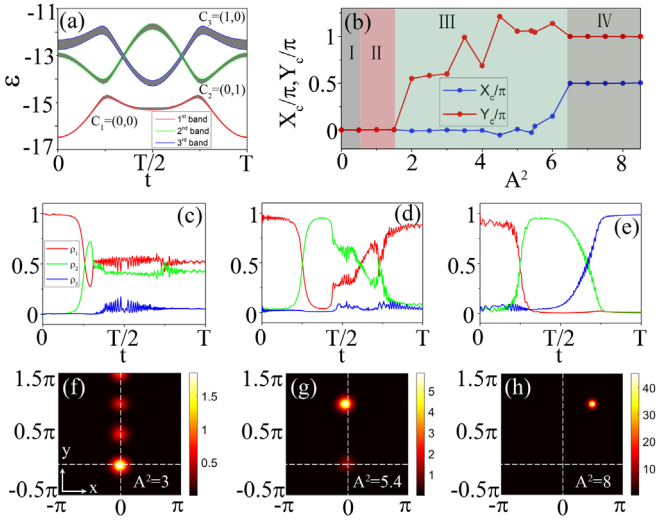

FIG. 3. (a) Evolution of 2D bands of the potential (4) with $\mathfrak{V}_x = 5$, $\mathfrak{v}_x = 1.2$, $\mathfrak{V}_y = 4.2$, $\mathfrak{v}_y = 2$ with $T = T_x = 2T_y$. (b) Center of mass coordinates at $t = T$. Different colors correspond to scenarios shown in Fig. 1(b). Evolution of populations ρ_1 (red), ρ_2 (green) and ρ_3 (blue) for $A^2 = 3$ (c), 5.4 (d) and 8 (e). (f)–(h) Distributions $|\Psi|^2$ at $t = T$ for the respective amplitudes. The initial conditions are the same as in Fig. 1.

located along the y axis at nearly equidistant points $y_n \approx n\pi/2$ (with $n = 0, 1, \ldots$).

Finally, in the domain ④ in Fig. 3(b) we again observe quantized transport carried by a large-amplitude soliton [Fig. 3(h)]. The one-cycle displacement of the soliton, $(\pi/2, \pi)$ in Fig. 3(h) can be understood using (3) if we consider it as a one-cycle shift of the second band soliton $\pi \boldsymbol{C}_2(T)$ over the one period of lattice in the y direction, i.e., at $T/2$ where only the second band is populated [green line in Fig. 3(e)], and subsequent displacement of the third-band soliton $\pi \boldsymbol{C}_3(T/2)$ [blue line in Fig. 3(e)] over a half-period of the x lattice.

We have described 2D nonlinear Thouless pumping of an attractive BEC in an adiabatically varying commensurate OL. The transport can occur in quasilinear, single-soliton, or multisoliton regimes. The scenario is determined by the dynamical Chern numbers of the linear bands and by the band populations affected by nonlinearity-induced interband tunneling. Single-soliton transport occurs for relatively small and high-amplitude wave packets. For amplitudes between these limits, the transport is carried by several solitons born upon the decay of the initial wave packet. The concept of 2D quantized transport remains meaningful also for nonequal commensurate temporal periods of the mutually orthogonal OLs. Nonlinear quantum transport in continuous lattices with incommensurate periods remains an open question.

Q. F., P. W., and F. Y. acknowledge support from NSFC (No. 91950120), Natural Science Foundation of Shanghai (No. 19ZR1424400), and Shanghai Outstanding Academic Leaders Plan (No. 20XD1402000). V. V. K. acknowledges financial support from the Portuguese Foundation for Science and Technology (FCT) under Contracts No. PTDC/FIS-OUT/3882/2020 and No. UIDB/00618/2020.

*Corresponding author.
fangweiye@sjtu.edu.cn

[1] D. J. Thouless, Quantization of particle transport, Phys. Rev. B **27**, 6083 (1983).
[2] Q. Niu and D. J. Thouless, Quantised adiabatic charge transport in the presence of substrate disorder and many-body interaction, J. Phys. A **17**, 2453 (1984).
[3] Q. Niu, Towards a Quantum Pump of Electric Charges, Phys. Rev. Lett. **64**, 1812 (1990).
[4] D. Xiao, M.-C. Chang, and Q. Niu, Berry phase effects on electronic properties, Rev. Mod. Phys. **82**, 1959 (2010).
[5] W. Ma, L. Zhou, Q. Zhang, M. Li, C. Cheng, J. Geng, X. Rong, F. Shi, J. Gong, and J. Du, Experimental Observation of a Generalized Thouless Pump with a Single Spin, Phys. Rev. Lett. **120**, 120501 (2018).
[6] S. Nakajima, T. Tomita, S. Taie, T. Ichinose, H. Ozawa, L. Wang, M. Troyer, and Y. Takahashi, Topological Thouless pumping of ultracold fermions, Nat. Phys. **12**, 296 (2016).
[7] S. Nakajima, N. Takei, K. Sakuma, Y. Kuno, P. Marra, and Y. Takahashi, Competition and interplay between topology and quasi-periodic disorder in Thouless pumping of ultracold atoms, Nat. Phys. **17**, 844 (2021).
[8] L. Taddia, E. Cornfeld, D. Rossini, L. Mazza, E. Sela, and R. Fazio, Topological Fractional Pumping with Alkaline-Earth-Like Atoms in Synthetic Lattices, Phys. Rev. Lett. **118**, 230402 (2017).
[9] M. Lohse, S. Schweizer, O. Zilberberg, M. Aidelsburger, and I. Bloch, A Thouless quantum pump with ultracold bosonic atoms in an optical superlattice, Nat. Phys. **12**, 350 (2016).
[10] M. Lohse, C. Schweizer, H. M. Price, O. Zilberberg, and I. Bloch, Exploring 4D quantum Hall physics with a 2D topological charge pump, Nature (London) **553**, 55 (2018).
[11] Y. E. Kraus, Y. Lahini, Z. Ringe, M. Verbin, and O. Zilberberg, Topological States and Adiabatic Pumping in Quasicrystals, Phys. Rev. Lett. **109**, 106402 (2012).
[12] O. Zilberberg, S. Huang, J. Guglielmon, M. Wang, K. P. Chen, Y. E. Kraus, and M. C. Rechtsman, Photonic topological boundary pumping as a probe of 4D quantum Hall physics, Nature (London) **553**, 59 (2018).
[13] A. Cerjan, M. Wang, S. Huang, K. P. Chen, and M. Rechtsman, Thouless pumping in disordered photonic systems, Light. Light. **9**, 178 (2020).
[14] W. Cheng, E. Prodan, and C. Prodan, Experimental Demonstration of Dynamic Topological Pumping across Incommensurate Bilayered Acoustic Metamaterials, Phys. Rev. Lett. **125**, 224301 (2020).
[15] Z. Fedorova, H. Qiu, S. Linden, and J. Kroha, Observation of topological transport quantization by dissipation in fast Thouless pumps, Nat. Commun. **11**, 3758 (2020).

[16] P. Wang, Q. Fu, R. Peng, Y. V. Kartashov, L. Torner, V. V. Konotop, and F. Ye, Two-dimensional Thouless pumping of light in photonic moiré lattices (to be published).
[17] F. Matsuda, M. Tezuka, and N. Kawakami, Two-dimensional Thouless pumping of ultracold fermions in obliquely introduced optical superlattice, J. Phys. Soc. Jpn. **89**, 114708 (2020).
[18] M. Nakagawa, T. Yoshida, R. Peters, and N. Kawakami, Breakdown of topological Thouless pumping in the strongly interacting regime, Phys. Rev. B **98**, 115147 (2018).
[19] Q. Fu, P. Wang, Y. V. Kartashov, V. V. Konotop, and F. Ye, Nonlinear Thouless Pumping: Solitons and Transport Breakdown, Phys. Rev. Lett. **128**, 154101 (2022).
[20] M. Jürgensen and M. C. Rechtsman, Chern Number Governs Soliton Motion in Nonlinear Thouless Pumps, Phys. Rev. Lett. **128**, 113901 (2022).
[21] N. Mostaan, F. Grusdt, and N. Goldman, Quantized Transport of Solitons in Nonlinear Thouless Pumpings: From Wannier Drags to Topological Polarons, arXiv:2110.08696.
[22] M. Jürgensen, S. Mukherjee, and M. C. Rechtsman, Quantized nonlinear Thouless pumping, Nature (London) **596**, 63 (2021).
[23] J. Tangpanitanon, V. M. Bastidas, S. Al-Assam, P. Roushan, D. Jaksch, and D. G. Angelakis, Topological Pumping of Photons in Nonlinear Resonator Arrays, Phys. Rev. Lett. **117**, 213603 (2016).
[24] T. Haug, R. Dumke, L.-C. Kwek, and L. Amico, Topological pumping in Aharonov—Bohm rings, Commun. Phys. **2**, 127 (2019).
[25] Y. Kuno and Y. Hatsugai, Interaction-induced topological charge pump, Phys. Rev. Res. **2**, 042024(R) (2020).
[26] L. Bergé, Wave collapse in physics: Principles and applications to light and plasma waves, Phys. Rep. **303**, 259 (1998).
[27] G. Fibich, *The Nonlinear Schrödinger Equation: Singular Solutions and Optical Collapse* (Springer, Heidelberg, 2015).
[28] B. B. Baizakov, B. A. Malomed, and M. Salerno, Multidimensional solitons in a low-dimensional periodic potential, Phys. Rev. A **70**, 053613 (2004).
[29] D. Mihalache, D. Mazilu, F. Lederer, Y. V. Kartashov, L.-C. Crasovan, and L. Torner, Stable three-dimensional spatiotemporal solitons in a two-dimensional photonic lattice, Phys. Rev. E **70**, 055603(R) (2004).
[30] W. Kohn, Analytic properties of Bloch waves and Wannier functions, Phys. Rev. **115**, 809 (1959).
[31] N. Marzari, A. A. Mostof, J. R. Yates, I. Souza, and D. Vanderbilt, Maximally localized Wannier functions: Theory and applications, Rev. Mod. Phys. **84**, 1419 (2012).
[32] See Supplemental Material at http://link.aps.org/supplemental/10.1103/PhysRevLett.129.183901, which includes Refs. [19,20,30,33], for derivation.
[33] G. L. Alfimov, P. G. Kevrekidis, V. V. Konotop, and M. Salerno, Wannier functions analysis of the nonlinear Schrödinger equation with a periodic potential, Phys. Rev. E **66**, 046608 (2002).
[34] R. D. King-Smith and D. Vanderbilt, Theory of polarization of crystalline solids, Phys. Rev. B **47**, 1651 (1993).
[35] B. B. Baizakov, B. A. Malomed, and M. Salerno, Multidimensional solitons in periodic potentials, Europhys. Lett. **63**, 642 (2003).
[36] B. B. Baizakov, B. A. Malomed, and M. Salerno, Multidimensional solitons in a low-dimensional periodic potential, Phys. Rev. A **70**, 053613 (2004).
[37] E. A. Donley, N. R. Claussen, S. L. Cornish, J. L. Roberts, E. A. Cornell, and C. E. Wieman, Dynamics of collapsing and exploding Bose-Einstein condensates, Nature (London) **412**, 295 (2001).
[38] R. A. Duine and H. T. C. Stoof, Explosion of a Collapsing Bose-Einstein Condensate, Phys. Rev. Lett. **86**, 2204 (2001).
[39] V. A. Yurovsky, Quantum effects on dynamics of instabilities in Bose-Einstein condensates, Phys. Rev. A **65**, 033605 (2002).